LETTER

In vitro Self-Assembly of Gold Nanoparticle-Coated Poly(3-hydroxybutyrate) Granules Exhibiting Plasmon-Induced Thermo-Optical Enhancements

Diego A. Rey,*,†,‡ Aaron D. Strickland,‡ Dickson Kirui,†,‡ Nuttawee Niamsiri,§ and Carl A. Batt‡

Graduate Field of Biomedical Engineering and Department of Food Science, Cornell University, Ithaca, New York, and Department of Biotechnology, Mahidol University, Bangkok, Thailand

ABSTRACT Polyhydroxyalkanoate (PHA) synthase attached to gold nanoparticles (AuNP) produce poly(3-hydroxybutyrate) (PHB) upon the addition of 3-hydroxybutyrate-CoA, and then coalesce to form micrometer-sized AuNP-coated PHB granules. These AuNP-coated PHB granules are potential theranostic agents that have enhanced imaging capabilities and are capable of heating upon near-infrared laser irradiation. The AuNP-coated PHB exhibited 11-fold enhancement in surface-enhanced Raman scattering over particles prior polymerization. Stained AuNP-coated PHB exhibited a 6-fold enhancement in fluorescence intensity as well as a 1.3-fold decrease in photobleaching rate compared to PHB granules alone. The granules were also shown to emit heat when illuminated at 808 nm with a 3.9-fold increase in heating rate compared to particles alone.

KEYWORDS: polyhydroxyalkanoate synthase • poly(3-hydroxybutyrate) • gold nanoparticles • self-assembly • surface enhanced Raman scattering • enhanced fluorescence • near-infrared • thermo-optical

INTRODUCTION

Polyhydroxyalkanoate (PHA) polyesters are a class of polymers that can be synthesized by many bacteria from (R)-3-hydroxyacyl-CoA as a stored carbon source produced under conditions of limited nutrients and excess carbon (1−12). PHA is stored as granular inclusions in the cytoplasm and can make up over 80% of a bacteria's dry weight (13). The primary enzyme involved in PHA synthesis is PHA synthase and the granules are accompanied by several additional 'granule associated proteins' (GAPs) that take part in PHA regulation. Two predominant models for in vivo granule formation have been proposed and structural characterization of the resulting granule has been reported (14, 15). During granule formation, PHA synthase binds its substrate and then dimerizes before elongation of the PHA chain. Because PHA is insoluble in water, the polymer begins to coalesce via hydrophobic interactions between the polymer chains. This results in a granular structure in which PHA synthase remains on the granule surface while the newly synthesized PHA is deposited into the granule core. PHA synthase is the only GAP that is required for granule formation, providing a straightforward means of producing PHA granules in vitro (16).

Recently, the use of PHA in its granule form has emerged as a promising new nanoparticle for a variety of applications; these advances have been recently reviewed (15). Functionalized PHA granules have been produced via in vivo self-assembly (in the bacterial host) employing GAP-fusion constructs including phasins and PHA synthase (17−26). In vitro approaches have decorated either extracted granules or granules synthetically produced from processed PHA using GAP-tagged proteins (27−30). An additional avenue for developing functional PHA nanoparticles has been accomplished through the chemical addition of functional groups on the PHA polymer chain (31, 32). More recently, functionalized PHB granules were produced via in vitro polymerization from genetically engineered PHA synthase fused to RGD peptides (33). These granules were shown to specifically bind to breast cancer cells that constitutively express $\alpha_v\beta_3$ integrins showing promise as a targeted drug-delivery agent. In general, modified PHA granules have shown promise as protein purification systems, immunodetection, and drug delivery (15, 33, 34).

Here we describe the development of gold nanoparticle (AuNP)-coated poly(3-hydroxybutyrate) (PHB) granules assembled via in vitro polymerization from AuNP-PHA synthase conjugates. PHB is formed from 3-hydroxybutyrate (3HB) and is among the most common PHAs. This approach was inspired by our prior work utilizing PHA synthase for enzymatic surface initiated polymerization (ESIP) for applications in bottom-up nano/microfabrication on a variety of micropatterned surfaces as well as on microbeads (11, 35−39). In this current study, we thought to expand our

* Corresponding author. Phone: (607) 255-7902. Fax: (607) 255-4884. E-mail: dr225@cornell.edu.

Received for review April 4, 2010 and accepted June 16, 2010

† Graduate Field of Biomedical Engineering, Cornell University.

‡ Department of Food Science, Cornell University.

§ Mahidol University.

DOI: 10.1021/am100306m

Published on Web 06/21/2010

repertoire of ESIP-derived structures by functionalizing gold nanoparticles with PHA synthase, providing a novel platform from which to polymerize PHB. Based on the natural PHB granules structure, those produced from nanoparticle-PHA synthase conjugates were expected to result in nanoparticle-coated granules that would lead to the possibility of exploiting effects caused by the nanoparticle arrangement on the granule surface. Transmission electron microscopy (TEM) analysis of PHB granules derived from AuNP conjugates revealed that the PHB granules were indeed coated with gold nanoparticles leading to exploring the potential of these constructs in exhibiting plasmon-induced phenomena such as Surface Enhanced Raman Scattering (SERS), fluorescence enhancement, and photothermal heating. These AuNP-coated PHB granules are shown to exhibit enhanced SERS and fluorescence as well as the capability of emitting heat from near-infrared (NIR) illumination. These properties may allow for the use of these granules as theranostic agents that may be followed via SERS and fluorescence and may deliver therapeutic payloads in the form of heat and as a PHB-mediated drug-delivery agent (32−34, 40).

EXPERIMENTAL SECTION

Gold nanoparticles were synthesized following Presa, et al.: mixing gold acetate $Au(ac)_3$, 1,2-hexadecanediol, and phenylether, and then heating to 80 °C under N_2 before adding oleic acid and oleylamine before refluxing at 260 °C for 30 min (41). The resulting oleic acid/oleylamine-coated AuNPs were made water-soluble following Dubertret, et al.: mixing AuNP-oleic acid/oleylamine with 1,2-distearoyl-sn-glycero-3-phosphoethanolamine-*N*-[carboxy(polyethylene glycol)2000] (PL-PEG-COOH) in chloroform, evaporating the chloroform, and reconstituting the particles in water to produce PL-PEG-COOH-coated AuNP (42). The carboxyl groups of the AuNP-PL-PEG-COOH were then converted to primary amine-reactive NHS-esters using 1-ethyl-3-[3-dimethylaminopropyl] carbodiimide hydrochloride (EDC) and *N*-hydroxysulfosuccinimide (sulfo-NHS) (Pierce Biotechnology, Rockford, IL) following the manufacturer's protocol. The AuNP-PL-PEG-NHS-ester particles were then mixed with PHA synthase in 50 mM Na-phosphate buffer at pH 7 at a 1:1 AuNP:PHA synthase mass-to-mass ratio and allowed to react for 2 h at room temperature, resulting in AuNP-PL-PEG conjugated to PHA synthase (AuNP-PHA synthase). PHA synthase functionalized particles were analyzed via dynamic light scattering (DLS) and TEM. Polymerization of PHB from the conjugates and the formation of PHB granules were confirmed via TEM and fluorescence microscopy of stained PHB.

To measure the SERS characteristics of AuNP-coated PHB granules, we added a solution of the Raman-active molecule phenyl disulfide in 50 mM sodium phosphate buffer, pH 7, to samples of AuNP-PHA synthase and AuNP-coated PHB at a final phenyl disulfide concentration of 1 mM. SERS analysis was performed using a Renishaw InVia microRaman system equipped with a 785 nm solid-state laser.

For enhanced fluorescence and photobleaching experiments, samples of AuNP-coated and uncoated PHB were stained with Nile red at a 1 μg/mL working concentration. Fluorescence measurements were conducted with an inverted fluorescence microscope, equipped with a 560 nm/645 nm excitation/emission filter cube, a 100× objective lens, and CCD camera. Images were captured at 1 s intervals for 30 s and analyzed using Image Pro Plus to determine PHB granule intensity.

Heating experiments were conducted using a 1.2 W, 808 nm continuous-wave diode laser culminated to a 0.5 mm diameter beam with temperature measurements conducted using a fiber optic temperature sensor. Thirty microliters of AuNP-PHA synthase, AuNP-coated PHB, and a reference sample of 50 mM sodium phosphate buffer, pH 7, were placed inside PCR tubes with the temperature probe positioned away from incident laser light. Samples were illuminated at 3 W/mm^2 and their temperature was monitored over a period of 2 min.

RESULTS AND DISCUSSION

Nanoparticle Functionalization and Granule Formation. DLS and TEM observations indicated that AuNP-PHA synthase particles consist of individual and unaggregated particles in solution (see Figure S1 in the Supporting Information). Starting with unaggregated AuNP-PHA synthase prior to polymerization allowed for studying aggregation-derived phenomena upon aggregation mediated by PHB polymerization. With the addition of 3HBCoA to AuNP-PHA synthase conjugates, PHB polymer was produced and grew to polydisperse spherical granules up to 1500 nm in diameter (Figure 1A). As can be seen in the TEM images, these granules are coated with AuNP particles that are observed as round structures with dark spots on their surface. The presence of PHB could also be observed by staining with Nile red and subsequently imaging the granules using fluorescence microscopy (Figure 1B). Nile red exhibits little fluorescence in hydrophilic mediums yet brightly fluoresces upon incorporation into hydrophobic matrices. The observation of Nile-red-stained granules via fluorescence microscopy indicates that these AuNP-coated granules maintain a hydrophobic core as in native PHB granules. The resulting nanoparticle coating is consistent with the proposed mechanism of PHB granule formation and a possible assembly mechanism based on this mechanism is diagramed in Figure 1C (14, 15).

Surface-Enhanced Raman Scattering. In this study, samples containing AuNP-coated PHB granules exhibited enhanced SERS signals over aggregated AuNP-PHA synthase particles. For example, at a dilution corresponding to an $OD_{520} = 0.016$ (1/5-fold dilution) samples containing only AuNP-PHA synthase exhibited little to no signal for adsorbed phenyl disulfide; however, samples containing both AuNP-PHA synthase and AuNP-coated PHB granules exhibited a relatively strong signal. When comparing the 1000 cm^{-1} (benzene ring vibration (43)) Raman band intensity of adsorbed phenyl disulfide, the average Raman intensity for the latter samples was 3983 counts over baseline (Figure 2A) with the average enhancement for samples containing

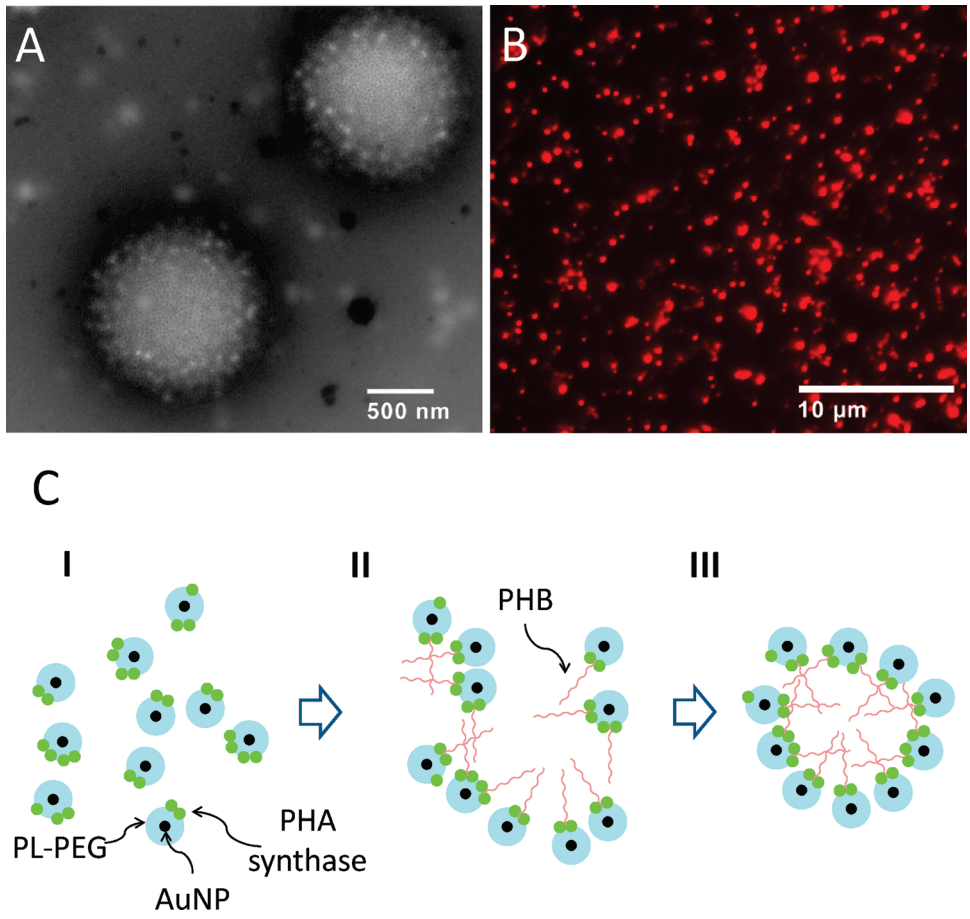

FIGURE 1. AuNP-coated PHB granules. (A) TEM image of AuNP-coated PHB granules. (B) Nile-red-stained, AuNP-coated PHB granules imaged at 100× magnification via fluorescence microscopy. (C) Proposed mechanism for AuNP-coated PHB granule formation: (I) PHA synthase is conjugated to AuNP. (II) In the presence of 3HBCoA, PHB polymer chains begin to form from PHA synthase dimers on the AuNP surface, causing the nanoparticles to coalesce via hydrophobic interactions among polymerizing PHB. (III) In this manner, the structures begin to take a granular form with AuNP remaining on the granule surface.

AuNP-coated PHB granules ranging from 3 ± 0.2 to 11 ± 0.81 across the dilutions tested (Figure 2B).

It is thought that the organization of gold nanoparticles around PHB granules gives rise to the observed SERS enhancement relative to the AuNP-PHA synthase conjugates. AuNP-PHB samples contained both AuNP-coated PHB granules as well as AuNP not associated with PHB granules (i.e., free AuNP-synthase conjugates). This is due to the fact that granule formation from the polymerization of AuNP-PHA synthase conjugates is not 100% efficient. Thus, the SERS signal observed from samples containing both AuNP-PHB and AuNP-PHA synthase arises from minimal enhancement due to inherent aggregation of AuNP-synthase conjugates upon drying the sample, and an apparent strong enhancement from the AuNP decorated PHB granules. This thesis is supported by the fact that little to no enhancement was observed for samples containing only aggregated AuNP-PHA synthase. This result indicates that enhancement in SERS is mediated by PHB polymerization and the formation of controlled AuNP aggregates on the surface of PHB granules, which are not present when AuNP aggregation is caused by the drying of AuNP-PHA synthase samples. The interparticle interactions on the PHB granule surface are likely to produce defined electromagnetic hot spots and this is thought to provide the dominant form of SERS enhancement (44−46). The shell structure that is formed by the nanoparticle coating may also contribute to the observed enhancement, as similar metallic shell structures have been shown to increase both the effective volume in which molecules are affected by the enhanced electric field and the Raman gain averaged over this volume (47).

Fluorescence Enhancement. When comparing AuNP-coated and uncoated, Nile-red-stained PHB granules, coated granules exhibited increased fluorescence intensity per unit area of the imaged granules with an average enhancement factor of 6.01 ± 1.47. A concern during these measurements was that a larger granule size would contribute to the appearance of fluorescence enhancement simply due to a larger Nile red loading capacity. In fact, plotting the fluorescent spot intensity vs size of fluorescently imaged granules reveals a linear increase in fluorescence intensity with increasing unit area. Nevertheless, enhancement in fluorescence intensity comparing nanoparticle-coated and uncoated granules is evident (Figure 2C).

To examine the photobleaching characteristics of coated and uncoated Nile red granules, the same individual fluorescent spots analyzed for fluorescence enhancement were

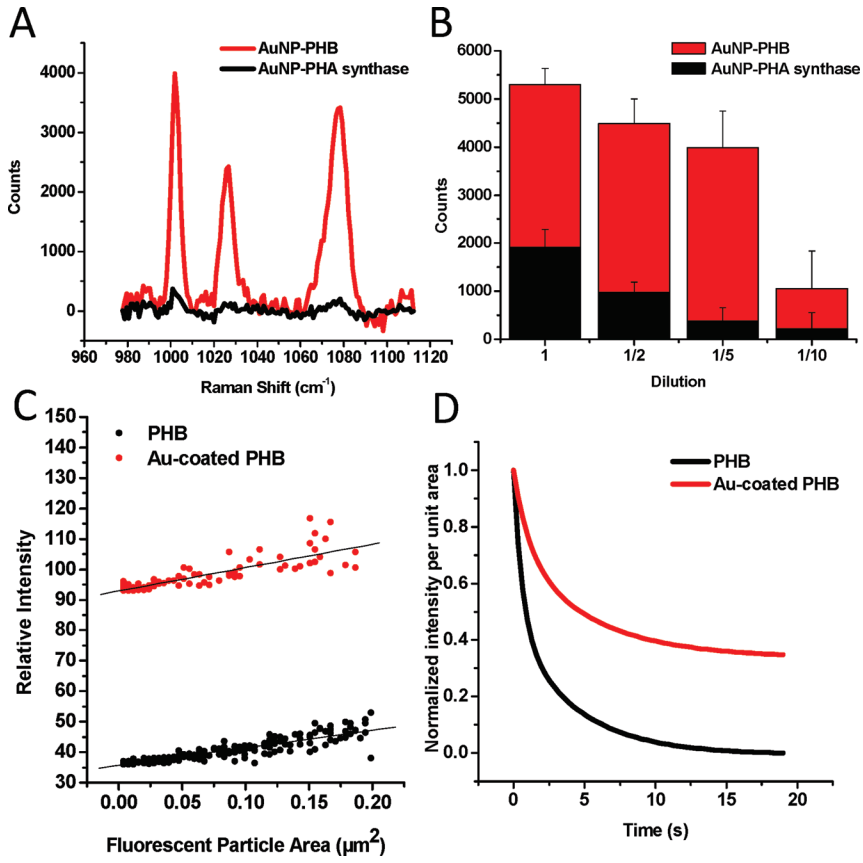

FIGURE 2. SERS and fluorescence enhancement from AuNP-coated PHB granules. (A, B) Enhanced SERS from AuNP-coated PHB granules vs AuNP-PHA synthase. The plot (A) shows the average Raman spectra for the sample at 1/5-fold dilution. The bar graph (B) shows the average number of counts and standard deviation for the 1000 cm^{-1} peak of phenyl disulfide. (C) Fluorescence intensity of AuNP-coated and uncoated PHB granules vs granule size. (D) Second-order exponential decay fits of the normalized average intensity per unit area vs time for AuNP-coated ($R^2 = 0.9995$) vs uncoated PHB ($R^2 = 0.9978$).

tracked and analyzed for fluorescence intensity per unit area in subsequent image sequences taken during continuous illumination by the microscope excitation source. Indeed, an increase in photo stability of Nile red was observed (Figure 2D) with a 1.3 ± 0.21-fold decrease in the fluorescence intensity decay rate for Au-coated PHB (0.16 ± 0.030 s^{-1}) compared to PHB alone (0.20 ± 0.015 s^{-1}).

The AuNP particle coating and their arrangement on the PHB granule surface reveals the likely source of fluorescent enhancement. Figure 3A depicts the possible AuNP-coated PHB granule geometry with regard to SERS and enhanced fluorescence. In the diagram, yellow stars represent Nile red that is shown to be incorporated in the hydrophobic PHB core as well as the hydrophobic layer comprised of the interface between the phospholipid tails of PL-PEG and oleic acid/oleylamine surrounding the AuNP. The blue stars represent Raman reporter molecules that similarly can become incorporated in these hydrophobic regions and can bind to the gold nanoparticle surface via its disulfide group (48). When a fluorophore is localized to metal particles or surfaces at less than ~5 nm, its emission is quenched by energy transfer to the metal (49). However, at further distances from the metal (between 5 and 70 nm), increases in fluorescence can be observed (49–52). While Nile red stains the PHB granule, it may also stain the hydrophobic layer around the AuNPs formed by the oleic acid/oleylamine and phospholipid. This layer, however, is less than 5 nm thick given our DLS particle size data and judging by the molecular dimensions of oleic acid, oleylamine, and the phospholipid (see Results in the Supporting Information). We have observed that Nile red within this layer is quenched by the gold nanoparticles (Figure 3B) (49). Quenching is expected because of the proximity of Nile red to the gold nanoparticle surface and because there is appreciable overlap between the extinction of the gold particles and the Nile red fluorescence spectrum (53). Conversely, given DLS measurements and the molecular dimensions of the nanoparticle coating (see Results in the Supporting Information), Nile red absorbed within the PHB granule is at a distance of at most ~25 nm from the gold particle (Figure 3A). Fluorescence enhancement has been observed between 5 and 70 nm away from nanostructured metallic surfaces, thus due to the configuration of AuNP-coated PHB granules, Nile red within the PHB granule is within a distance where enhanced fluorescence is possible (53). Furthermore, two phenomena can contribute to fluorescent enhancement including surface enhanced fluorescence (SEF) in which the metal particles concentrate the local excitation intensity and metal enhanced fluorescence (MEF) in which the electric field felt by a fluorophore is affected by interaction of the fluorophore oscillating dipole with the metal surface (52, 54–56). In MEF, an increase in the radiative rate is expected, resulting in an

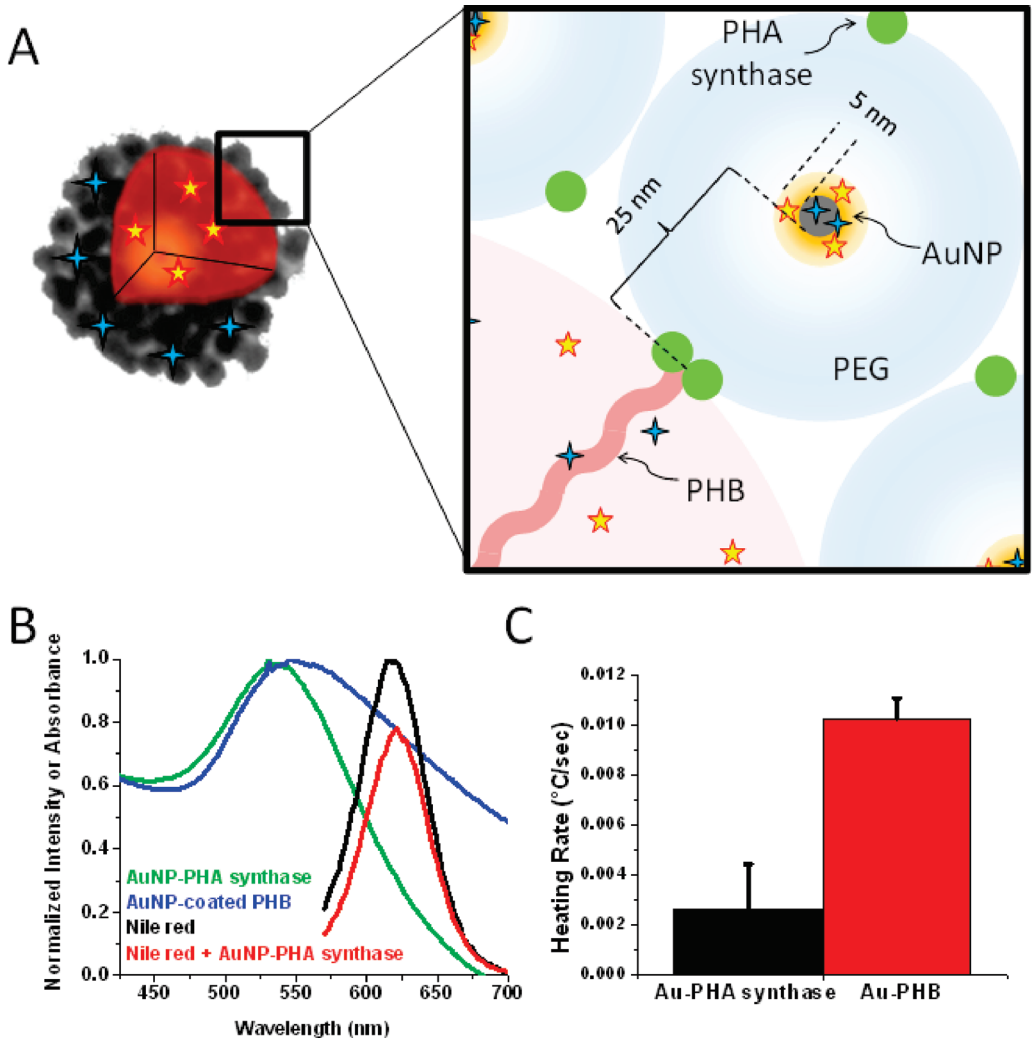

FIGURE 3. (A) Diagram of possible AuNP-coated PHB granule geometry with regard to SERS and enhanced fluorescence. Yellow stars represent Nile red and blue stars represent Raman reporter molecules. (B) Absorption spectra of AuNP-PHA synthase and AuNP-coated PHB superimposed with the emission spectra of Nile red fluorescence and quenched Nile red fluorescence due to the addition of AuNP-PHA synthase. (C) Average heating rate and standard deviation of AuNP-PHA synthase vs AuNP-coated PHB upon NIR illumination.

increased intensity and decrease in photobleaching since the fluorophore spends less time in the excited state for each excitation. Our observation of increased photo stability points to the possibility that the nanoparticle coating causes a decrease in the radiative decay rate of the Nile red, indicating that MEF contributes to fluorescence enhancement in the system.

NIR Heating. NIR-induced heating of AuNP-PHA synthase and AuNP-coated PHB granules resulted in a linear temperature increase for each sample with all measurements exhibiting an R^2 value greater than 0.997 for linear fits of the data. The 808 nm NIR laser illumination of AuNP-coated PHB granules resulted in a 3.9 ± 0.69 increase in the heating rate when compared to AuNP-PHA synthase prior to polymerization (Figure 3C), as determined from the slopes of the fitted temperature vs time plots. Due to the arrangement of the gold nanoparticles on the PHB granule surface, broadening in the plasmon resonance of the AuNP-coated PHB granules over AuNP-PHA synthase was observed (Figure 3B) and the increase in heating rate is likely due to increased overlap between the 808 nm laser source and the plasmon of the AuNP-coated PHB granules (57, 58).

CONCLUSIONS

In this work, AuNP-PHA synthase conjugates were constructed and shown to actively polymerize PHB. These nanoparticle conjugates consist of unaggregated AuNP. PHB polymerization from these conjugates resulted in AuNP-coated PHB granules offering a new means for producing functionalized PHB particles. When compared to AuNP-PHA synthase conjugates, the AuNP-coated PHB granules exhibited enhancement in SERS properties as well as increased heating rate upon NIR illumination. Nile red-stained AuNP-coated PHB granules also exhibited enhanced fluorescence and decreased photobleaching when compared to uncoated PHB granules.

Multimodal particles exhibiting various imaging and therapeutic characteristics are emerging as promising platforms in biomedical applications. In particular, the applicability of dual SERS/MEF particles in multiplexed immunoassays was recently shown (59). Furthermore, several studies have

demonstrated the utility of gold nanoparticle-based SERS imaging in vivo highlighting the advantages of high signal strength as well as the use of these materials as dual imaging and photothermal agents (60−65). Given the advances in utilizing PHB as a matrix for drug-delivery, our AuNP-PHA synthase conjugates may also serve as multimodal imaging/drug delivery vehicles in which gold-coated PHB granules carrying a drug and/or fluorophore may be tracked via fluorescence or SERS and may be heated via NIR illumination (33, 34, 40, 61, 62). In comparison to previously described dual SERS/MEF particles that were constructed via layer-by-layer deposition of polyelectrolyte coatings on silica cores, our AuNP-coated PHB offer a facile self-assembly approach for particle formation (59). Furthermore, the biodegradability and biocompatibility of PHB may facilitate the in vivo application of AuNP-coated PHB granules (66). On the other hand, synthetic means for particle synthesis often allow for greater control of particle size and polydispersity, a characteristic that few studies have addressed for PHB granule biosynthesis (33, 67). Ongoing studies by our laboratory aim to employ the nanoparticle-coated PHB granules developed here in diagnostic and therapeutic applications.

Acknowledgment. The work described was supported by Award F31CA130144 from the National Cancer Institute. The content is solely the responsibility of the authors and does not necessarily represent the official views of the National Cancer Institute or the National Institutes of Health.

Supporting Information Available: Experimental details regarding expression and purification of PHA synthase, size-exclusion chromatography, synthesis of 3HBCoA, synthesis of gold nanoparticles, functionalization of gold nanoparticles, AuNP-PL-PEG-COOH quantification, in vitro polymerization of 3HBCoA, dynamic light-scattering measurements, transmission electron microscopy, particle size analysis, Raman spectroscopy, fluorescence and extinction measurements and analysis, as well as result details regarding sSynthesis of AuNP, functionalization of AuNP, and selectivity of AuNP-PL-PEG-COOH toward nonpolar SERS reporters (PDF). This material is available free of charge via the Internet at http://pubs.acs.org.

REFERENCES AND NOTES

(1) Brandl, H.; Gross, R. A.; Lenz, R. W.; Fuller, R. C. *Appl. Environ. Microbiol.* **1988**, *54*, 1977–1982.
(2) Han, J.; Lu, Q.; Zhou, L.; Zhou, J.; Xiang, H. *Appl. Environ. Microbiol.* **2007**, *73*, 6058–6065.
(3) Hezayen, F. F.; Rehm, B. H. A.; Eberhardt, R.; Steinbüchel, A. *Appl. Microbiol. Biotechnol.* **2000**, *54*, 319–325.
(4) Hezayen, F. F.; Steinbüchel, A.; Rehm, B. H. A. *Arch. Biochem. Biophys.* **2002**, *403*, 284–291.
(5) Hezayen, F. F.; Tindall, B. J.; Steinbüchel, A.; Rehm, B. H. A. *Int. J. Syst. Evol. Bacteriol.* **2002**, *52*, 2271–2280.
(6) Lu, Q.; Han, J.; Zhou, L.; Zhou, J.; Xiang, H. *J. Bacteriol.* **2008**, *190*, 4173–4180.
(7) Dai Gao, A. M.; Yamane, T.; Ueda, S. *FEMS Microbiol. Lett.* **2001**, *196*, 159–164.
(8) Handrick, R.; Reinhardt, S.; Jendrossek, D. *J. Bacteriol.* **2000**, *182*, 5916–5918.
(9) Ou, J. T.; Reim, R. L. *J. Bacteriol.* **1978**, *133*, 442–445.
(10) Hoffmann, N.; Rehm, B. H. A. *Biotechnol. Lett.* **2005**, *27*, 279–282.
(11) Kim, Y.; Paik, H.; Ober, C.; Coates, G.; Mark, S.; Ryan, T.; Batt, C. *Macromol. Biosci.* **2006**, *6*, 145–152.
(12) Kuchta, K.; Chi, L.; Fuchs, H.; Potter, M.; Steinbuchel, A. *Biomacromolecules* **2007**, *8*, 657–662.
(13) Madison, L. L.; Huisman, G. W. *Microbiol. Mol. Biol. Rev.* **1999**, *63*, 21–53.
(14) Stubbe, J.; Tian, J. *Nat. Prod. Rep.* **2003**, *20*, 445–457.
(15) Grage, K.; Jahns, A. C.; Parlane, N.; Palanisamy, R.; Rasiah, I. A.; Atwood, J. A.; Rehm, B. H. A. *Biomacromolecules* **2009**, *10*, 660–669.
(16) Gerngross, T. U.; Martin, D. P. *Proc. Natl. Acad. Sci. U.S.A.* **1995**, *92*, 6279–6283.
(17) Banki, M.; Gerngross, T.; Wood, D. *Protein Sci.* **2005**, *14*, 1387–1395.
(18) Barnard, G. C.; McCool, J. D.; Wood, D. W.; Gerngross, T. U. *Appl. Environ. Microbiol.* **2005**, *71*, 5735–5742.
(19) Peters, V.; Rehm, B. H. A. *FEMS Microbiol. Lett.* **2005**, *248*, 93–100.
(20) Peters, V.; Rehm, B. H. A. *Appl. Environ. Microbiol.* **2006**, *72*, 1777–1783.
(21) Brockelbank, J. A.; Peters, V.; Rehm, B. H. A. *Appl. Environ. Microbiol.* **2006**, *72*, 7394–7397.
(22) Grage, K.; Rehm, B. H. A. *Bioconjugate Chem.* **2008**, *19*, 254–262.
(23) Peters, V.; Rehm, B. H. A. *J. Biotechnol.* **2008**, *134*, 266–274.
(24) Backstrom, B. T.; Brockelbank, J.; Rehm, B. *BMC Biotechnol.* **2007**, *7*, 3.
(25) Jahns, A. C.; Haverkamp, R. G.; Rehm, B. H. A. *Bioconj. Chem.* **2008**, *19*, 2072–2080.
(26) Atwood, J.; Rehm, B. *Biotechnol. Lett.* **2009**, *31*, 131–137.
(27) Moldes, C.; Garcia, P.; Garcia, J. L.; Prieto, M. A. *Appl. Environ. Microbiol.* **2004**, *70*, 3205–3212.
(28) Wang, Z.; Wu, H.; Chen, J.; Zhang, J.; Yao, Y.; Chen, G. *Lab Chip* **2008**, *8*, 1957–1962.
(29) Lee, S. J.; Park, J. P.; Park, T. J.; Lee, S. Y.; Lee, S.; Park, J. K. *Anal. Chem.* **2005**, *77*, 5755–5759.
(30) Ihssen, J.; Magnani, D.; Tholn̈y-Meyer, L.; Ren, Q. *Biomacromolecules* **2009**, *10*, 1854−1864.
(31) Sparks, J.; Scholz, C. *Biomacromolecules* **2008**, *9*, 2091–2096.
(32) Sparks, J.; Scholz, C. *Biomacromolecules* **2009**, *10*, 1715–1719.
(33) Han-Nah Kim, J. L.; Kim, H.-Y.; Kim, Y.-R. *Chem. Commun.* **2009**, 7104–7106.
(34) Xiong, Y. C.; Yao, Y. C.; Zhan, X. Y.; Chen, G. Q. *J. Biomater. Sci., Polym. Ed.* **2010**, *21*, 127–140.
(35) Kim, Y. P., H.; Ober, C. K.; Coates, G. W.; Batt, C. A. *Biomacromolecules* **2004**, *5*, 889–894.
(36) Kim, Y.-R.; Paik, H.-j.; Ober, C. K.; Batt, C. A. *Polym. Prepr.* **2002**, *43*, 706–707.
(37) Kim, Y.-R.; Paik, H.-j.; Ober, C. K.; Coates, G. W.; Batt, C. A. *Polym. Prepr. (Am. Chem. Soc., Div. Polym. Chem.)* **2002**, *43*, 706–707.
(38) Niamsiri, N.; Bergkvist, M.; Delamarre, S. C.; Cady, N. C.; Coates, G. W.; Ober, C. K.; Batt, C. A. *Colloids Surf., B* **2007**, *60*, 68–79.
(39) Paik, H. J.; Kim, Y. R.; Orth, R. N.; Ober, C. K.; Coates, G. W.; Batt, C. A. *Chem. Commun.* **2005**, 1956–1958.
(40) Pouton, C. W.; Akhtar, S. *Adv. Drug Delivery Rev.* **1996**, *18*, 133–162.
(41) De la Presa, P.; Multigner, M.; De la Venta, J.; Garcia, M. A.; Ruiz-Gonzalez, M. L. *J. Appl. Phys.* **2006**, *100*, 123915.
(42) Dubertret, B.; Skourides, P.; Norris, D. J.; Noireaux, V.; Brivanlou, A. H.; Libchaber, A. *Science* **2002**, *298*, 1759–1762.
(43) Dai, Q. P.; Xue, C. C.; Xue, G.; Jiang, L. X. *J. Adhes. Sci. Technol.* **1995**, *9*, 1465–1474.
(44) Braun, G.; Pavel, I.; Morrill, A. R.; Seferos, D. S.; Bazan, G. C.; Reich, N. O.; Moskovits, M. *J. Am. Chem. Soc.* **2007**, *129*, 7760-+.
(45) Basu, S.; Pande, S.; Jana, S.; Bolisetty, S.; Pal, T. *Langmuir* **2008**, *24*, 5562–5568.
(46) Xu, H.; Aizpurua, J.; Käll, M.; Apell, P. *Phys. Rev. E* **2000**, *62*, 4318.
(47) Simovski, C. R. *Phys. Rev. B* **2009**, *79*, 5.
(48) Hickman, J. J.; Ofer, D.; Zou, C. F.; Wrighton, M. S.; Laibinis, P. E.; Whitesides, G. M. *J. Am. Chem. Soc.* **1991**, *113*, 1128–1132.
(49) Kummerlen, J.; Leitner, A.; Brunner, H.; Aussenegg, F. R.; Wokaun, A. *Mol. Phys.* **1993**, *80*, 1031–1046.
(50) Glass, A. M.; Liao, P. F.; Bergman, J. G.; Olson, D. H. *Opt. Lett.* **1980**, *5*, 368–370.
(51) Campion, A.; Gallo, A. R.; Harris, C. B.; Robota, H. J.; Whitmore, P. M. *Chem. Phys. Lett.* **1980**, *73*, 447–450.
(52) Sokolov, K.; Chumanov, G.; Cotton, T. M. *Anal. Chem.* **1998**, *70*, 3898–3905.

(53) Lakowicz, J. R. *Principles of Fluorescence Spectroscopy*; Springer Science+Business Media: New York, 2006.
(54) Hayakawa, T.; Selvan, S. T.; Nogami, M. *Appl. Phys. Lett.* **1999**, *74*, 1513–1515.
(55) Selvan, S. T.; Hayakawa, T.; Nogami, M. *J. Phys. Chem. B* **1999**, *103*, 7064–7067.
(56) Lakowicz, J. R. *Anal. Biochem.* **2001**, *298*, 1–24.
(57) Phadtare, S.; Kumar, A.; Vinod, V. P.; Dash, C.; Palaskar, D. V.; Rao, M.; Shukla, P. G.; Sivaram, S.; Sastry, M. *Chem. Mater.* **2003**, *15*, 1944–1949.
(58) Ji, T.; Avny, Y.; Davidov, D. *Mater. Res. Soc. Symp. Proc.* **2001**, *636*.
(59) Kim, K.; Lee, Y. M.; Lee, H. B.; Shin, K. S. *ACS Appl. Mater. Interfaces* **2009**, *1*, 2174–2180.
(60) Geoffrey von, M.; Andrea, C.; Ji-Ho, P.; Renuka, R.; Michael, J. S.; Hatton, T. A.; Sangeeta, N. B. *Adv. Mater.* **2009**, *21*, 3175–3180.
(61) Kirui, D. K.; Rey, D. A.; Batt, C. A. *Nanotechnology* **2010**, *21*, 105105.
(62) Lal, S.; Clare, S. E.; Halas, N. J. *Acc. Chem. Res.* **2008**, *41*, 1842–1851.
(63) Qian, X. M.; Peng, X. H.; Ansari, D. O.; Yin-Goen, Q.; Chen, G. Z.; Shin, D. M.; Yang, L.; Young, A. N.; Wang, M. D.; Nie, S. M. *Nat. Biotechnol.* **2008**, *26*, 83–90.
(64) Xiao, M.; Nyagilo, J.; Arora, V.; Kulkarni, P.; Xu, D.; Sun, X.; Dave, D. P. *Nanotechnology* **2010**, *21*, 035101.
(65) Zavaleta, C. L.; Smith, B. R.; Walton, I.; Doering, W.; Davis, G.; Shojaei, B.; Natan, M. J.; Gambhir, S. S. *Proc. Natl. Acad. Sci. U.S.A.* **2009**, *106*, 13511–13516.
(66) Martin, D. P.; Williams, S. F. *Biochem. Eng. J.* **2003**, *16*, 97–105.
(67) Jossek, R.; Reichelt, R.; Steinbüchel, A. *Appl. Microbiol. Biotechnol.* **1998**, *49*, 258–266.

AM100306M